Computational Modeling Analysis of a Spinal Cord Stimulation Paddle Lead Reveals Broad, Gapless Dermatomal Coverage

Alexander R. Kent, Xiaoyi Min, Stuart P. Rosenberg, and Timothy A. Fayram

Abstract— **Spinal cord stimulation (SCS) is an effective therapy for treating chronic pain. The St. Jude Medical PENTA™ paddle lead features a 4×5 contact array for achieving broad, selective coverage of dorsal column (DC) fibers. The objective of this work was to evaluate DC activation regions that correspond to dermatomal coverage with use of the PENTA lead in conjunction with a lateral sweep programming algorithm. We used a two-stage computational model, including a finite element method model of field potentials in the spinal cord during stimulation, coupled to a biophysical cable model of mammalian, myelinated nerve fibers to determine fiber activation within the DC. We found that across contact configurations used clinically in the sweep algorithm, the activation region shifted smoothly between left and right DC, and could achieve gapless medio-lateral coverage in dermatomal fiber tract zones. Increasing stimulation amplitude between the DC threshold and discomfort threshold led to a greater area of activation and number of dermatomal zones covered on the left and/or right DC, including L1-2 zones corresponding to dermatomes of the lower back. This work demonstrates that the flexibility in contact selection offered by the PENTA lead may enable patient-specific tailoring of SCS.**

I. Introduction

Spinal cord stimulation (SCS) is an established therapy for treatment of chronic pain of the back and limbs. The SCS lead is placed in the dorsal epidural space and is connected to an implanted pulse generator (IPG) placed in a subcutaneous location that delivers electrical current through the lead to the spinal cord. This current generates field potentials within the spinal cord, and supra-threshold potentials drive generation of action potentials in nerve fibers. The therapeutic mechanism of action of SCS is thought to be based on Melzack and Wall's "gate-control theory," in which activation of large, myelinated mechanoreceptor afferents (Aβ fibers) in the spinal cord indirectly modulates painful sensory signals carried by smaller, unmyelinated afferents (C fibers) via local circuit neurons in the dorsal horn [1]. Electrical stimulation of Aβ fibers in the dorsal column (DC) suppresses pain and generates coincident paresthesia in dermatomal body regions that are innervated by these DC fiber tracts, which are hereafter referred to as "dermatomal zones."

Research supported by St. Jude Medical.

A. R. Kent is with St. Jude Medical, Sunnyvale, CA 94085 USA (e-mail: akent02@sjm.com).

X. Min is with St. Jude Medical, Sylmar, CA 91342 USA (e-mail: xmin@sjm.com).

S. P. Rosenberg is with St. Jude Medical, Sylmar, CA 91342 USA (e-mail: srosenberg@sjm.com).

T. A. Fayram is with St. Jude Medical, Sunnyvale, CA 94085 USA (e-mail: tfayram@sjm.com).

Paddle-type SCS leads provide a means to optimize paresthesia coverage of painful dermatomal areas and thereby achieve patient-specific tailoring. These leads are characterized by a multi-contact array fixed to an insulating lead body that promotes uni-directional current flow into the spinal cord. For example, the St. Jude Medical PENTA paddle lead is designed with a 4×5 contact array and 9 mm wide lead body that enables broad lateral coverage. This lead can be used in conjunction with a lateral sweep programming algorithm, which steps through various anode-cathode contact configurations. Together, these features are intended to provide flexible and gapless coverage in medio-lateral current steering across the DC with the use of a single current source IPG. The objective of this work was to locate activation regions within the DC and determine dermatomal zone coverage across contact configurations and stimulation intensities through the use of computer simulation.

II. Methods

This study used a computational model of SCS to calculate neuronal activation within the DC with stimulation by the St. Jude Medical PENTA paddle lead.

A two-stage model was developed for calculating the effect of SCS on DC fiber activation within the spinal cord, based on a similar approach taken by Holsheimer and colleagues at the University of Twente [2]. The first stage was a three-dimensional volume conductor model used to calculate electrical field potentials in the lower thoracic spinal column generated by SCS (Section A). The output of the volume conductor model was coupled to the second stage, which was a biophysical model of mammalian, myelinated nerve fibers, and was used to identify fibers in the DC population that were activated by SCS (Section B).

A. Volume Conductor Model

The volume conductor model was built using ANSYS Maxwell 3D, a finite element method (FEM) modeling software package, to calculate the electrical fields generated

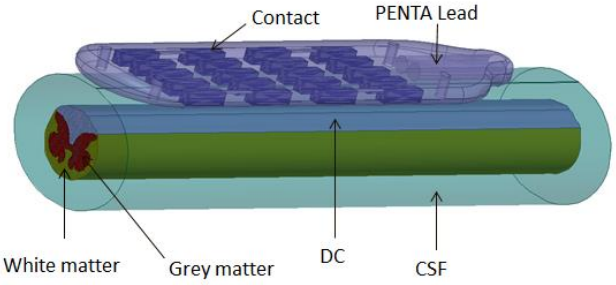

Figure 1. Three-dimensional representation of the FEM model geometry, including spinal cord, CSF, and PENTA lead in the epidural space.

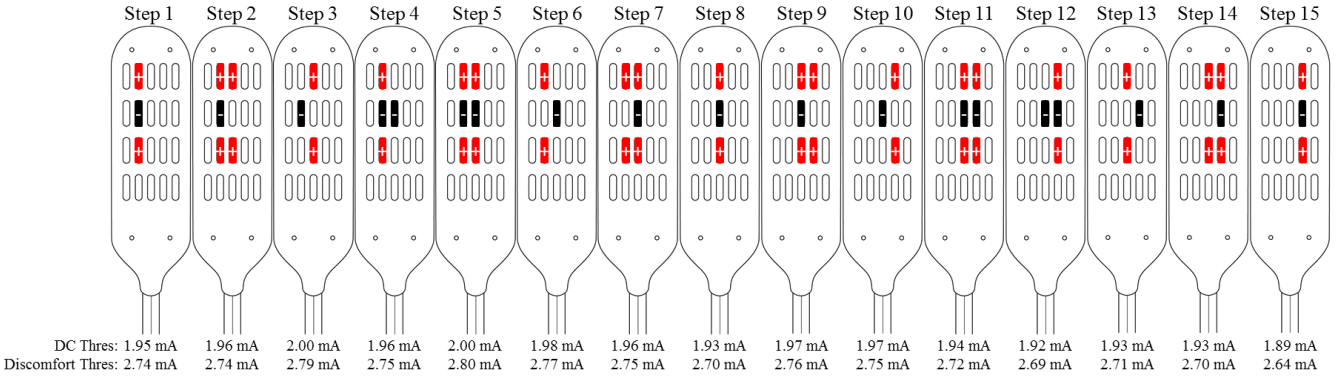

Figure 2. *Top*: Diagram of the fifteen tripolar contact configurations (steps) tested with the PENTA lead. Thirteen steps are available in the Rapid Programmer™, and two were added for this study (steps 4 and 12). Cathodic (negative) contacts are shown in black and anodic (positive) contacts in red. *Bottom*: DC and discomfort thresholds across the 15 contact configuration steps.

by SCS (Fig. 1). We modeled the anatomical and conductive properties of the lower thoracic (T7-T10) spinal cord. The subdomains represented in the FEM model were: spinal cord gray matter (conductivity of 0.25 S/m), DC and other white matter (anisotropic conductivity; 0.72 S/m in longitudinal direction, 0.083 S/m in transverse direction), 3.2 mm thick cerebrospinal fluid layer (CSF, 1.67 S/m), epidural fat (0.05 S/m), and vertebral bone (0.025 S/m) [3, 4]. Additionally, the PENTA lead was placed symmetrically over the spinal cord within the dorsal epidural space. The lead has an array of 16 independent, conductive Pt/Ir contacts and a silicone rubber insulating body. The contacts are 1×4 mm in size with 1 mm edge-to-edge lateral spacing and 3 mm longitudinal spacing. The contacts in the outer columns are wired together in pairs for optional anodal stimulation.

Tripolar contact configurations were established by setting cathodes and anodes with a 1 V boundary condition in the FEM model, and calculating the corresponding stimulation current. We studied the contact configurations available in the lateral sweep algorithm and which are used in the clinical setting (MultiSteering™ Technology available in the Rapid Programmer™ System). These configurations are shown in Fig. 2. Since the FEM boundary value problem was linear in this model, the field potentials generated by a given configuration with particular stimulation current amplitude could be calculated as a scaled version of the original solution. These field potentials were exported for coupling to the second stage of the model, described in Section B.

B. Biophysical Model of Myelinated Nerve Fibers

The neuronal response to stimulation within the DC was investigated using the Sweeney model of a mammalian, myelinated nerve fiber [5], built in NEURON v7.3. This model features segments representing nodes of Ranvier and adjacent myelinated internodes, with all segments connected by an intracellular conductivity (Fig. 3). Node of Ranvier segments contain transmembrane sodium ion and leakage currents in parallel with membrane capacitance, and the internodal myelin sheath is modelled as perfectly insulating (no transmembrane current flow). The equations and parameters describing this cable-based model are provided in [6]. This model provides a computationally-efficient approach for calculating spinal cord fiber thresholds [7].

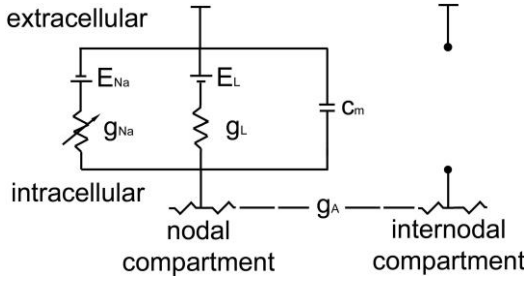

Figure 3. Diagram of the Sweeney model, a biophysical cellular model of nerve fibers within the DC. The nodes of Ranvier are represented by sodium ion (conductance g_{Na} and Nernst potential E_{Na}) and leakage (g_L and E_L) currents in parallel with membrane capacitance (c_m), and are connected to perfectly insulating internodal segments via an intracellular conductance (g_A).

The DC was populated with representative model nerve fibers. In the transverse cross-section, fibers were arranged in a grid distribution with a density of 400 fibers/mm^2. Longitudinally, each fiber was oriented in the same direction as the dorsal column. The internode segment length in this direction was 1.2 mm, with a randomized longitudinal location of the first node of each axon. Other fiber dimensions were 12 µm internode diameter, 7.2 µm node diameter, and 1.5 µm node length [8, 9].

Controlled-current stimulation was delivered to the fibers of the DC and activation areas were identified. The FEM field potentials were interpolated at the nodes of Ranvier of a given fiber, and after scaling the magnitude of the potentials according to the stimulation current amplitude specified for testing, were applied extracellularly in the NEURON model. The stimulation waveform was a cathodic step pulse with 100 µs duration and was delivered with a 100 µs delay after

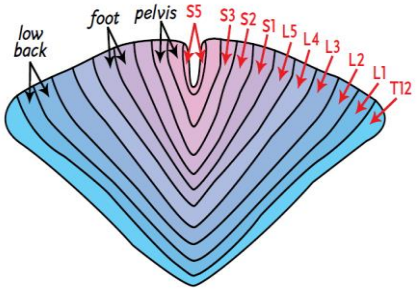

Figure 4. DC dermatomal zone map at the T11 level of the spinal cord. Image used with permission from [11].

the start of the simulation to allow for initialization to steady state. The total duration of the simulation was 2 ms to observe the full response of a given fiber following the stimulation pulse. Fiber activation was identified through measurement of transmembrane potential (V_M) at the middle node of each fiber and defining a threshold of $V_M \geq$ -20 mV for excitation [10]. For each contact configuration, we defined the DC threshold as the minimum stimulation amplitude that activated just one fiber in the DC and the discomfort threshold as 140% of the DC threshold [3, 8, 12]. Finally, we calculated the DC activation regions (area of activated fibers) across stimulation amplitudes for each contact configuration, and mapped this to dermatomal zones using an established template (Fig. 4). Gapless coverage was defined as a maximum shift of one dermatomal zone (left or right DC) between two adjacent contact configuration steps.

III. Results

The DC and discomfort thresholds across contact configurations are provided in Fig. 2. The mean DC threshold was 1.95 ± 0.03 mA (average ± SD, range: 1.89 – 2.00 mA) and mean discomfort threshold was 2.73 ± 0.04 mA (range: 2.64 – 2.80 mA). The difference in thresholds observed for mirror-image configurations (e.g., steps 1 and 15) resulted from the asymmetrical geometry of the DC. The mean impedance across configurations was 160 ± 29 Ω (range: 110 – 204 Ω).

We calculated the area of activation in the DC for three stimulation current amplitudes between the DC and discomfort thresholds (2.2, 2.4, and 2.6 mA). DC activation regions are shown at 2.6 mA across contact configurations in Fig. 5. The region of activation shifted smoothly from the left to right DC as the contact configuration was changed from step 1 through step 15. Dermatomal zone mapping showed gapless coverage with 2.6 mA amplitude across configurations (Table 1). Depending on the configuration, 13 to 14 zones were concomitantly activated at 2.6 mA, ranging from the left L1 to the right L1 dermatomes.

Decreasing the stimulation current amplitude from 2.6 mA to 2.4 or 2.2 mA led to a reduced area of activation within the DC (Fig. 6). This decreased the total number of dermatomal zones activated on the left and/or right DC by 1 to 3 zones with 2.4 mA, and a further loss of 2 to 3 zones at 2.2 mA (Table 1). Depending on the configuration, 10 to 13 zones were concomitantly activated at 2.4 mA, and 8 to 11 zones at 2.2 mA. Importantly, gapless coverage was also observed at both 2.2 and 2.4 mA (Table 1).

IV. Discussion

We suggest that this computational modeling analysis provides several clinically relevant insights into the activation of DC fibers during SCS by the PENTA lead.

First, by varying contact configurations and/or stimulation current amplitudes, the PENTA lead can achieve broad, gapless coverage of dermatomal zones in a selective manner. Stepping through contact configurations using the lateral sweep programming algorithm shifted dermatomal zones on the left or right side of the DC by one zone at a time. Eliminating larger jumps in dermatomal zones may allow for discrete targeting by clinicians. In addition, incrementally increasing the stimulation current amplitude by only 0.2 mA expanded activation by 1 to 3 dermatomal zones in the left and/or right DC, depending on the contact configuration. Therefore, adjustment of stimulation amplitude within the range set by the DC threshold and discomfort threshold provides another means for discrete targeting of dermatomal zones. Overall these results indicate that the configuration flexibility provided by the 16 independent contacts on the PENTA lead, used in conjunction with a single current source IPG and a lateral sweep algorithm, can be used to tailor SCS therapy to patient clinical requirements by matching paresthesia coverage with the sites of pain. This flexibility could be particularly important in accounting for variation in patient spinal cord anatomy.

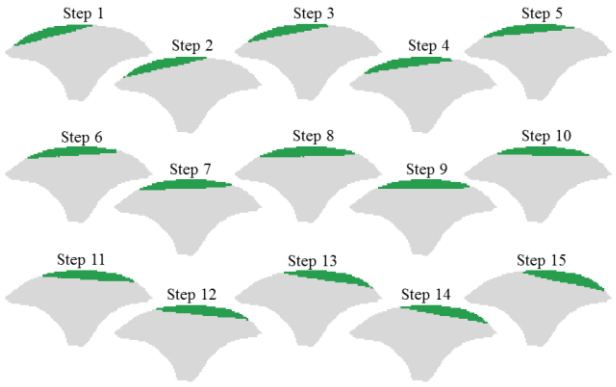

Figure 5. Activation regions (green fill) in DC at 2.6 mA across the 15 contact configuration steps.

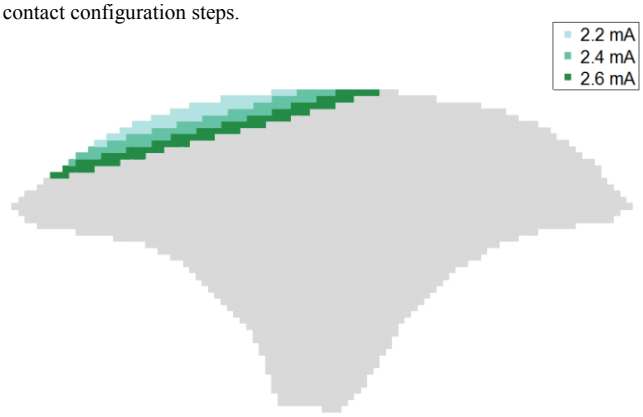

Figure 6. DC activation regions with step 1 configuration across the three stimulation current amplitudes tested, differentiated by fill colors. Note that activation regions for higher amplitudes encompass those regions activated at lower amplitudes.

Second, the PENTA lead is effective in activating the L1 and L2 dermatomal zones in the left and right DC, which innervate the lower back. These were generally activated at higher amplitudes (2.4 or 2.6 mA) using steps 1 to 4 for the left zones and steps 12 to 15 for the right zones. Therefore, the PENTA array appears well-suited for treating patients with lower back pain.

In this study, we measured nerve fiber responses to single stimulation pulses, but believe these results are applicable to tonic stimulation at clinical frequencies (~50 Hz). Activated

Table 1. Mapped dermatomal zone activation across the 15 contact configuration steps, with mapped regions extending from left to right L1 zones. Activation is shown for the three tested stimulation current amplitudes, 2.2 mA (■), and additional dermatomal zone activation with increasing of amplitude to 2.4 mA (■) and then to 2.6 mA (■). In some cases, dermatomal zone activation was unchanged on the left or right side with an incremental increase in stimulation amplitude (e.g., right zones unchanged with step 13 for an increase from 2.4 to 2.6 mA).

Contact Configuration	Left Zones										Right Zones									
	L1	L2	L3	L4	L5	S1	S2	S3	S4	S5	S5	S4	S3	S2	S1	L5	L4	L3	L2	L1
Step 1																				
Step 2																				
Step 3																				
Step 4																				
Step 5																				
Step 6																				
Step 7																				
Step 8																				
Step 9																				
Step 10																				
Step 11																				
Step 12																				
Step 13																				
Step 14																				
Step 15																				

fibers recover to baseline within 1 ms, which is well within the inter-pulse interval (~20 ms) of a typical stimulus train, suggesting comparable fiber recruitment with each pulse.

V. Conclusion

Computer simulations indicate that use of the PENTA paddle lead, combined with a lateral sweep algorithm, can provide broad, gapless coverage of dermatomes in a selective manner. The flexibility in contact configuration selection may allow for tailoring of therapy to patient needs through paresthesia-pain area convergence. These results warrant further clinical investigation.

References

[1] R. Melzack and P. D. Wall, "Pain mechanisms: a new theory," *Science*, vol. 150, no. 3699, pp. 971-979, Nov. 1965.

[2] J. J. Struijk and J. Holsheimer, "Transverse tripolar spinal cord stimulation: theoretical performance of a dual channel system," *Med. Biol. Eng. Comput.,* vol. 34, no. 4, pp. 273-279, Jul. 1996.

[3] J. Holsheimer and W. A. Wesselink, "Optimum electrode geometry for spinal cord stimulation: the narrow bipole and tripole," *Med. Biol. Eng. Comput.,* vol. 35, no. 5, pp. 493-497, 1997.

[4] J. Holsheimer, J. A. den Boer, J. J. Struijk, and A. R. Rozeboom, "MR assessment of the normal position of the spinal cord in the spinal canal," *AJNR Am. J. Neuroradiol.,* vol. 15, pp. 951-959, May 1994.

[5] J. D. Sweeney, J. T. Mortimer, and D. Durand, "Modeling of mammalian myelinated nerve for functional neuromuscular electrostimulation," *IEEE 9th Annu. Conf. Eng. Med. Biol. Soc.*, pp. 1577-1578, 1987.

[6] C. C. McIntyre and W. M. Grill, "Sensitivity analysis of a model of mammalian neural membrane," *Biol. Cybern.,* vol. 79, no. 1, pp. 29-37, Jul. 1998.

[7] F. Rattay, K. Minassian, and M. R. Dimitrijevic, "Epidural electrical stimulation of posterior structures of the human lumbosacral cord: 2. Quantitative analysis by computer modeling," *Spinal Cord*, 38(8): 473-489, Aug. 2000.

[8] D. Lee, B. Hershey, K. Bradley, and T. Yearwood, "Predicted effects of pulse width programming in spinal cord stimulation: a mathematical modeling study," *Med. Biol. Eng. Comput.*, 49(7): 765-774, Jul. 2011.

[9] E. N. Warman, W. M. Grill, and D. Durand, "Modeling the effects of electric fields on nerve fibers: determination of excitation thresholds," *IEEE Trans. Biomed. Eng.*, vol. 39, no. 12, Dec. 1992.

[10] A. R. Kent and W. M. Grill. "Model-based analysis and design of nerve cuff electrodes for restoration of bladder function by selective stimulation of the pudendal nerve," *J. Neural Eng.*, vol. 10, no. 3, pp. 1-15, Apr. 2013.

[11] H. K. Feirabend, H. Choufoer, S. Ploeger, J. Holsheimer, and J. D. van Gool, "Morphometry of human superficial dorsal and dorsolateral column fibres: significance to spinal cord stimulation," *Brain,* vol. 125 (pt. 5), pp. 1137-1149, May 2002.

[12] M. A. Moffitt, D. C. Lee, and K. Bradley, "Spinal Cord Stimulation: Engineering Approaches to Clinical and Physiological Challenges," in Implantable Neural Prostheses 1: devices and applications, D.D. Zhou, E. Greenbaum, Eds. Springer Science + Business Media, 2009, pp. 155–194.